Journal of Power Sources 271 (2014) 48–54

Contents lists available at ScienceDirect

Journal of Power Sources

journal homepage: www.elsevier.com/locate/jpowsour

Thermal parameters determination of battery cells by local heat flux measurements

K.A. Murashko [a, *], A.V. Mityakov [a], J. Pyrhönen [a], V.Y. Mityakov [b], S.S. Sapozhnikov [b]

[a] Lappeenranta University of Technology LUT, Skinnarilankatu 34, 53850 Lappeenranta, Finland
[b] Saint-Petersburg State Polytechnical University, Polytechnicheskaya, 29, 195251 Saint-Petersburg, Russia

HIGHLIGHTS

- The methodology for measuring of the Li-ion cell thermal parameters was presented.
- The methodology was verified on the sample with well-known thermal parameters.
- The uncertainty and limitations for the presented methodology were given.
- The thermal parameters dependance on SoC and measuring points was studied.

ARTICLE INFO

Article history:
Received 5 May 2014
Received in revised form
25 June 2014
Accepted 19 July 2014
Available online 6 August 2014

Keywords:
Thermal parameters
Pouch cell
Li-ion battery
Heat flux sensor
Thermal model

ABSTRACT

A new approach to define of the thermal parameters, such as heat capacity and through-plane thermal conductivity, of pouch-type cells is introduced. Application of local heat flux measurement with a gradient heat flux sensor (GHFS) allows determination of the cell thermal parameters in different surface points of the cell. The suggested method is not cell destructive as it does not require deep discharge of the cell or application of any charge/discharge cycles during the measurements of the thermal parameters of the cell. The complete procedure is demonstrated on a high-power lithium-ion (Li-ion) pouch cell, and it is verified on a sample with well-known thermal parameters. A comparison of the experimental results with conventional thermal characterization methods shows an acceptably low error. The dependence of the cell thermal parameters on the state of charge (SoC) and measurement points on the surface was studied by the proposed measurement approach.

1. Introduction

General interest in high energy efficiency and in low emissions is increasing the popularity of different hybrid machines utilizing high-power electrical systems [1]. In applications of this kind, large battery cells with high power handling capability are typically needed. The battery, also, faces higher losses, which increase the temperature rise during cell operation. The operation of a cell in a high temperature accelerates the ageing of the cell and may increase the gasification process inside of the cell, which may violate the shell integrity and, in the worst case, lead to fire [2].

The traditional way of the thermal protection of the cell, which is based on the cell surface temperature measurements, may lead to overshoot of the maximum allowed temperature of the cell because of the thermal inertia of the system. Therefore, the thermal control of a cell, which is based on the prediction of the maximum temperature and the thermal gradients inside the cell, may give more safety in the thermal protection of the cell.

The prediction of the cell temperature requires application of the cell thermal model, which includes information about the thermal conductivity and heat capacity of the cell. The thermal modelling of the cell is discussed extensively in the literature (e.g. Refs. [3–23]). However, information about the thermal parameters of the cell is not easily available, as these parameters depend on the chemical processes, which occur during battery operation and lead to changing of the battery performance. For example if any gasification process occurs in a cell it will increase the volume of the cell and cause changes of the cell thermal conductivity and heat capacity. Increasing of the SEI layer during battery operation may lead to changing of the cell thermal parameters, too. Therefore, in-situ measurements of the cell thermal parameter are important with purpose to improve modelling of the cell or operation of the battery thermal management system. The specific heat capacity and thermal conductivity can be calculated as in Ref. [8]; however, it

* Corresponding author. Tel.: +358465733832.
E-mail address: kirill.murashko@lut.fi (K.A. Murashko).

http://dx.doi.org/10.1016/j.jpowsour.2014.07.117
0378-7753/

requires detailed information about the cell structure, which is normally confidential information and hence usually not available. Therefore, experimental methods for the determination of the cell thermal parameters are preferred.

In previous studies, the specific heat capacity was measured in calorimeter [19,24]. The measurement process requires that a deeply discharged cell can be heated in a liquid bath in a Dewar vessel, and the specific heat capacity of the cell is calculated based on the relation between the heating required energy and the temperature rise of the liquid.

The thermal conductivity and specific heat capacity can be measured by using an internal thermocouple as it was done in Ref. [20]. However, it requires using current pulses, and the thermal parameters of the cell are measured like lumped parameters. Another way to measure the thermal parameters of the cell is the Thermal Impedance Spectroscopy (TIS). TIS was applied to the thermal characterization of the Li-ion cell in Ref. [21] by using an external heat source for the generation of heat pulses to the surface of the cell and measuring the temperature behaviour of the cell. Also, internal power losses were used for the thermal characterization of the cell in Refs. [22] and [23]. However, such methods require expensive equipment and a special form of heat generation in the cell, and the experiments are very time consuming.

In this paper, a novel method is suggested for the determination of the heat capacity and through-plane thermal conductivity. The method is based on applying of gradient heat flux sensors (GHFSs) dedicated to the measurement of the heat flux. The method provides an opportunity to determine the thermal conductivity of the pouch cells in direction, which is perpendicular to the current collector, and the specific heat capacity by a single experiment. The experiment does not require steady-state mode at a certain temperature. Therefore, the cell thermal parameters can be determined in a short period of time. The presented method is applied here only for the experimental analysis of an L-ion pouch cell. The application of this method for other types of the cell is not considered in this article. In the method, a simple external heat source is used. The incoming and out-coming heat fluxes are measured by two GHFSs. The temperature is measured by temperature sensors placed in the proximity of the GHFSs. A comparison of the experimental results with actual values shows acceptable uncertainty in thermal parameter determination.

2. Methodology for thermal parameters determination

2.1. Li-ion pouch cell

A high power Li-ion pouch cell with dimensions 256 mm × 259 mm × 12.7 mm (width × height × thickness) was chosen for the determination of the thermal parameters. The Li-ion pouch cell was first presented in 1995. The typical structure of the Li-ion pouch cell is shown in Fig. 1.

The Li-ion pouch cell consists of N units. Each unit comprises two current collectors, a negative electrode, a positive electrode, and a separator, which is used for the mechanical separation of the negative and positive electrodes with the purpose to prevent short-circuit. The current collectors are used on both sides of each unit. As one current collector is used for two similar electrodes, the amount of the current collectors in the cell decreases, which in it turn reduces losses in the cell. The negative electrode is usually made from graphite. The positive electrode is made from metal oxide, for example lithium cobalt dioxide ($LiCoO_2$), lithium nickel manganese oxide ($LiNi_{0.5}Mn_{1.5}O_4$), or lithium iron phosphate ($LiFePO_4$). The separator is usually made from polymer, and it is permeable to an electrolyte in order to maintain the desired ionic conductivity. Usually, an organic carbonate solution electrolyte ($LiFP_6$) is used in

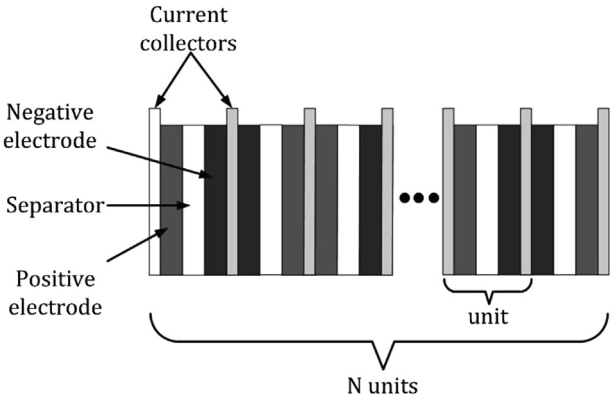

Fig. 1. Structure of the Li-ion pouch cell under study.

Li-ion cells. The current collector for the positive electrode is usually made from aluminium. The material for the current collector of the negative electrode depends on its properties. If graphite is used as the material for the negative electrode, then the current collector for this electrode is made from copper. However, in this work, a lithium titanate (LTO) cell is considered as the test cell. In this cell, lithium titanate oxide ($Li_4Ti_5O_{12}$) is used instead of graphite as the material for the negative electrode, which provides an opportunity to use aluminium, instead of copper, as the material for the negative current collector. The cathode material for the cell used in the verification process is lithium manganese spinel.

The thickness of the pouch cell is usually much smaller than the dimensions of the flat surface, which is parallel to the current collectors. This fact with the presented structure of the pouch cell provides an opportunity to consider a pouch LTO cell as an infinite plate with anisotropic thermal properties.

2.2. Determination of the thermal parameters in an infinite plate

The determination of the thermal parameters in an infinite plate can be considered a one-dimensional task, if a uniform heat flux through the plate is generated. Because of anisotropy of the pouch cell the one-dimensional temperature gradient should be established in directions that are perpendicular or parallel to the largest surface area of the cell. In this case, the one dimensional heat flux is expected and the thermal parameters of the cell can be determined in these directions.

In this work, the determination of the thermal parameters is performed in the direction perpendicular to the current collectors. The LTO pouch cell is considered an infinite plate as shown in Fig. 2(a).

During the experiment the initial temperature is equal to T_0 in each point of the cell. The boundary conditions are:

$$-k\cdot\left.\frac{\partial T}{\partial x}\right|_{x=0} = q_{\mathrm{th1}}(t) \tag{1}$$

$$-k\cdot\left.\frac{\partial T}{\partial x}\right|_{x=h} = q_{\mathrm{th2}}(t), \tag{2}$$

where k is the heat transfer coefficient (W m^{-1} K^{-1}), T is temperature (K), and $q_{\mathrm{th1}}(t)$, and $q_{\mathrm{th2}}(t)$ are the time-dependent heat fluxes (W m^{-2}).

The calculation of the thermal conductivity and specific heat capacity is based on the measured data and the equations, which are given below.

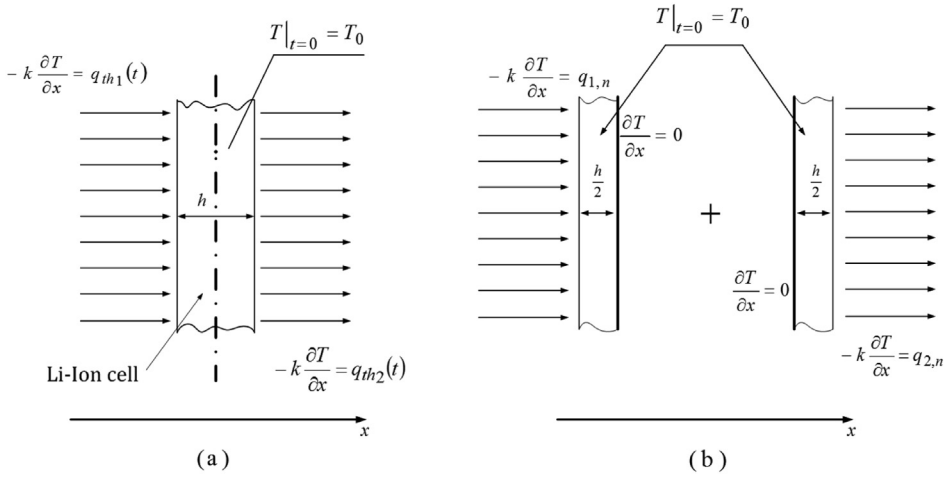

Fig. 2. Pouch LTO cell (a) and division into two elementary tasks (b) during the calculation of the thermal parameters.

For the sake of simplicity, the measured input and output heat flux curves are divided into small time intervals τ_n, in which the values of the heat fluxes are assumed constant and equal to the average values of the heat flux in these intervals. According to the superposition principle, the temperature in the plate can be calculated by a sum of N tasks with constant average values of the heat flux, where N is the number of considered intervals. Also, we can assume that in the middle of the plate in an infinitesimal range the temperature gradient is equal to zero [25,26]. Therefore, according to the superposition principle, each N task can be divided into two elementary tasks (Fig. 2(b)), in which only half plate with one thermally insulated side is considered. Therefore, according to the methodology presented in Ref. [25] the temperature for each point of the plate and average temperature in the plate are calculated as a sum of $2N$ elementary tasks by Eqs. (3) and (4),correspondingly.

$$T_x = T_0 + \mathbf{\Theta}(\eta_-) \times \mathbf{Q}_1 \cdot \frac{h}{k} - \mathbf{\Theta}(\eta_+) \times \mathbf{Q}_2 \cdot \frac{h}{k}, \tag{3}$$

$$\overline{T} = T_0 + \frac{2 \cdot \mathbf{V} \times \mathbf{Q}_1}{C_p \cdot \rho \cdot h} - \frac{2 \cdot \mathbf{V} \times \mathbf{Q}_2}{C_p \cdot \rho \cdot h}, \tag{4}$$

where $\mathbf{Q}_1$ and $\mathbf{Q}_2$ are $1 \times N$ matrices, that include the input and output heat flux average values q_1 and q_2, respectively, $\mathbf{V}$ is the $N \times 1$ matrix, that include time intervals τ_n (s), h is the thickness of the cell (m), ρ is the density (kg m^{-3}) and C_p is the specific heat capacity (J kg^{-1} K^{-1}), and $\mathbf{\Theta}$ is the $N \times 1$ matrix of the temperature coefficients, which depend on the dimensionless thickness coefficients η_- and η_+.

The dimensionless thickness coefficients are calculated as in Ref. [25]

$$\eta_- = \frac{x}{h} \tag{5}$$

$$\eta_+ = \frac{h - x}{h}, \tag{6}$$

where x is the distance from the plate surface where the heat flux penetrates the plate to the point in which the temperature is calculated (m), "−" and "+" denote the first and second elementary task, respectively.

The elements of $\mathbf{Q}_1$ and $\mathbf{Q}_2$ matrices are obtained as differences between the average values of the heat fluxes in the considered interval and the average values of the heat fluxes in the previous interval.

The elements of the $\mathbf{\Theta}$ matrix are obtained by the same way as in Ref. [25] at linear temperature gradient in the plate.

$$\mathbf{\Theta}_n = \mathrm{Fo}_n - \eta + \frac{\eta^2}{2} + \frac{1}{3}, \tag{7}$$

where Fo_n is the thermal Fourier number of the layer n, where $n = 1 \ldots N$ indicates the index of the considered interval.

According to [26] thermal Fourier numbers are calculated as.

$$\mathrm{Fo}_n = \frac{\alpha \cdot \tau_n}{h^2}, \tag{8}$$

where α is the thermal diffusivity (m^2 s^{-1}), which is calculated as in Ref. [26]

$$\alpha = \frac{k}{\rho \cdot C_p}, \tag{9}$$

The equation for the calculation of the specific heat capacity by using measured values of temperature and heat flux in points $x = 0$ and $x = h$ is obtained by simple transformation of the Eq. (4).

$$C_p = \frac{2 \cdot (\mathbf{V} \times \mathbf{Q}_1 - \mathbf{V} \times \mathbf{Q}_2)}{\rho \cdot h \cdot (\overline{T} - T_0)}, \tag{10}$$

The average temperature is calculated at leaner temperature gradient as.

$$\overline{T} = \frac{T|_{x=0} + T|_{x=h}}{2}, \tag{11}$$

The equation for the calculation of the thermal conductivity is obtained by substitution of the Eqs. (5)–(9) in Eq. (3). By transformation of the Eq. (3) the thermal conductivity is calculated for the points $x = 0$ and $x = h$ as.

$$k|_{x=0} = \frac{-h^2 \cdot C_p \cdot \rho \cdot \left(2 \cdot \sum_{n=1}^{N} q_{1n} + \sum_{n=1}^{N} q_{2n}\right)}{6 \cdot (\mathbf{V} \times \mathbf{Q}_1 - \mathbf{V} \times \mathbf{Q}_2 - C_p \cdot \rho \cdot h \cdot (T|_{x=0} - T_0))} \tag{12}$$

$$k|_{x=h} = \frac{h^2 \cdot C_p \cdot \rho \cdot \left(\sum_{n=1}^{N} q_{1n} + 2 \cdot \sum_{n=1}^{N} q_{2n} \right)}{6 \cdot (\mathbf{V} \times \mathbf{Q}_1 - \mathbf{V} \times \mathbf{Q}_2 - C_p \cdot \rho \cdot h \cdot (T|_{x=h} - T_0))} \quad (13)$$

The average value of the thermal conductivity is determined as.

$$k = \frac{k|_{x=0} + k|_{x=h}}{2} \quad (14)$$

2.3. Limitations

The following limitations for the application of Eqs. (10)–(14) should be considered before performing the experiment and calculation of the thermal parameters:

1. The cross-sectional area, which is perpendicular to the current collectors, should be much smaller than the cross-sectional area which is parallel to the current collectors. In this case, an infinite plate can be considered for the calculation of the necessary parameters.
2. The heat flux through the area, which is parallel to the current collectors, should be uniform. This requirement is necessary for the simplification of the calculation and reduction of the considered task to a one-dimensional task.
3. An analysis of the experimental results and calculation of the thermal parameters should be performed at a linear temperature gradient in the heat flux direction.

The last requirement is necessary for the simplification of the calculation process. At a linear temperature gradient, the average temperature in the plate can be easily calculated, and Eqs. (10)–(14) can be used. The minimum time of the experiment after which the temperature gradient in the object becomes linear can be calculated by.

$$\tau_{min} = \frac{Fo_{min} \cdot h_s^2}{\alpha_s}, \quad (15)$$

where Fo_{min} is the minimum value of the Fourier numbers at which the temperature gradient in the object becomes linear, and h_s and α_s are the thickness and thermal diffusivity of the considered object, respectively.

The minimum value of the Fourier numbers is obtained by an analysis of the temperature gradient in the considered elementary task. The temperature gradient can be calculated as in Ref. [25].

$$\frac{\partial T}{\partial x} = -G \cdot \frac{q_{th}}{k}, \quad (16)$$

where G is dimensionless temperature gradient coefficient, q_{th} is the constant heat flux.

By neglecting the change in the thermal parameter values in the material, which is caused by the temperature gradient, we can assume that the form of the temperature gradient depends only on the temperature gradient coefficient, which is calculated as in Ref. [25].

$$G = 1 - \eta + \sum_{i=1}^{\infty} C_i \cdot \sin[\mu_i \cdot (1 - \eta)] \cdot \exp\left(-\mu_i^2 \cdot Fo\right), \quad (17)$$

where C_i and μ_i are the dimensionless parameter, which are calculated as

$$C_i = (-1)^{i+1} \cdot \frac{2}{\mu_i}, \quad (18)$$

$$\mu_i = i \cdot \pi, \quad (19)$$

The analysis of the dependence between the temperature gradient coefficient and Fo and the dimensionless thickness coefficient, presented in Fig. 3, shows that the temperature gradient coefficient will have a linear dependence on the dimensionless thickness coefficient if Fo > 0.5. Therefore, the linear temperature gradient in the infinite plate will be at Fo > 0.5, and the minimum time in which the analyses of the experiment results and the calculation of the thermal parameters are performed can be calculated at $Fo_{min} = 0.5$.

3. Test equipment

The presented methodology shows the necessity of the information about temperature and heat flux, and therefore, this information was obtained by using temperature sensors and GHFSs.

3.1. Gradient heat flux sensor

The operation of the GHFSs, which were used in the experiments, is based on the transverse Seebeck effect, in which the thermo-electromotive force (thermo-EMF) is proportional to the temperature gradient in the direction normal to the applied heat flux vector.

$$E = S \cdot \nabla T, \quad (20)$$

where S is the Seebeck tensor (V K^{-1}) and ∇T is the temperature gradient (K m^{-1}).

The GHFS used for the heat flux measuring in this paper was made of a material with a strong anisotropy of thermal conductivity, electric conductivity, and thermo-EMF. Because of anisotropy, in said sensors the temperature gradients, which are proportional to the electric field vector, are created in two directions: along and across to the applied heat flux [27]. In this case, the signal strength is proportional to the length of the sensor instead of the sensor thickness as in thermocouple sensors, since it is the main direction of the electric field vector in GHFS. Therefore, the sensor can be made as thin as possible to achieve fast response time and still maintains sufficient signal strength.

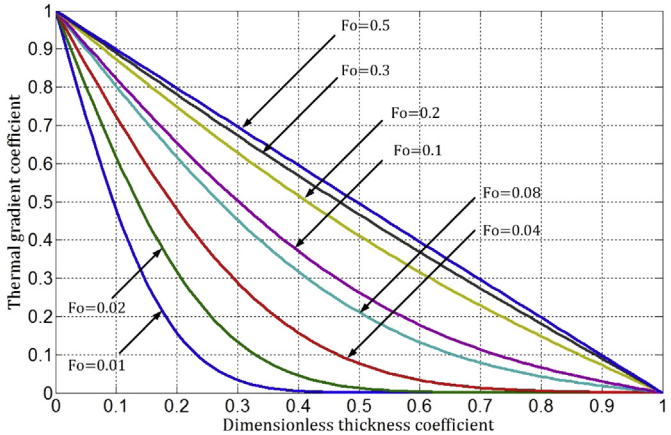

Fig. 3. Dependence of the thermal gradient coefficient on Fo and the dimensionless thickness coefficient.

The sensor used in this work was made from bismuth single crystals. Its design is shown in Fig. 4. More information about GHFS and its calibration can be found e.g. in Refs. [27–29].

The dimensions of the GHFS in the plane area are 5 × 20 mm, and the thickness is 0.15 mm. The heat flux per unit area of the sensor is determined as.

$$q_z = \frac{e}{b \cdot l_d \cdot S_0}, \tag{21}$$

where e is the thermo-EMF generated by the sensor (V), S_0 is the sensitivity (V W^{-1}), b and l_d are the sensor width and length (m), respectively.

The response time of the GHFS is extremely fast, about 10^{-8}–10^{-9} s, and it is independent of the sensor thickness [29].

3.2. Experimental setup

According to the presented methodology, the thermal parameters of the considered cell can be measured by performing a simple experiment, which is shown in Fig. 5.

Temperature and heat flux sensors were installed on both sides of the cell by using Dow corning 340 high thermal conductivity paste whose thermal conductivity equals to 0.586 W m^{-1} K^{-1}. The cell with sensors is squeezed by two aluminium plates, which increase the uniformity of the heat flux. Vacuum rubber is placed between the cell and the aluminium plates in order to compensate surface imperfections and remove air between the aluminium plates and the pouch cell. As vacuum rubber has a low thermal conductivity, the other surfaces of the cell, which are not in contact with the vacuum rubber, are thermally insulated by fibre glass. This is necessary for the generation of the heat flux only in one direction through the aluminium plates, vacuum rubber, and pouch cell.

A 500 W electric incandescent strip tube bulb is used to produce the heat flux through the system. The aluminium plate, closest to the lamp, was painted black to increase its emissivity. The signals from the temperature sensors are measured by a Fluke Hydra Series II meter, and the signals from the heat flux sensors are measured by a 34420A nanoVolt/micro-Ohm meter. All data are saved on a personal computer, and data processing is performed in Matlab.

An electric incandescent strip tube bulb can be used as a constant heat flux source, and as we are interested in the processes that occur before the second vacuum rubber, the thermal diffusivity can be calculated from Eq. (9) for the elements of the system before the second vacuum rubber with purpose to determine the minimum time of the experiment. As the constant heat flux passes

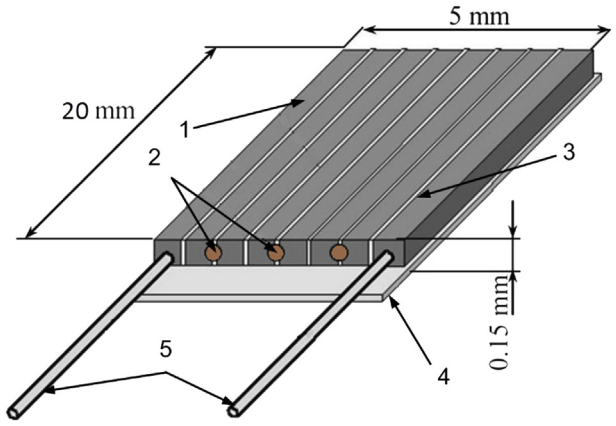

Fig. 4. GHFS: 1: bismuth thermoelement, 2: mica base, 3: solderings, 4: connecting wires, 5: insulation.

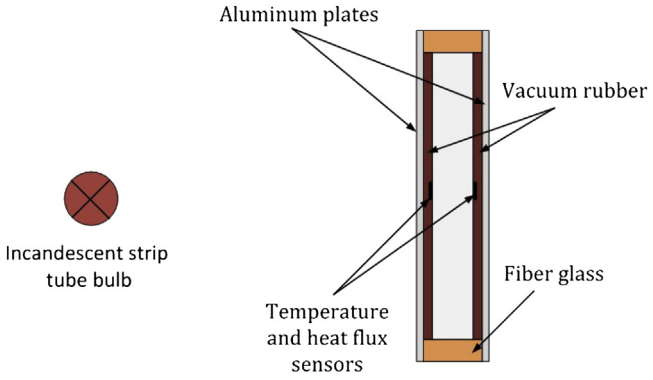

Fig. 5. Test setup.

successively through the aluminium plate, the vacuum rubber, and the considered cell in the test, the total values of k, ρ, and C_p are determined according to the methodology suggested in Ref. [8].

3.3. Uncertainty

The uncertainty was calculated according to EA-4/02 M: 2013. The standard uncertainty for the single measured value is calculated as.

$$u^2(y) = \sum_{i=1}^{N} \left(\frac{\partial f}{\partial x_i} \cdot u(x_i) \right)^2, \tag{22}$$

where $u(y)$ is the uncertainty of the output estimate y, $u(x_i)$ is the uncertainty of the input estimate x_i, where i is the number of the input estimates $i = 1 \ldots N$, and f is the function that shows the dependence between the input and the output.

According to Eqs. (10)–(14), the uncertainty of the determination of the thermal parameters depends on the uncertainty of the temperature sensors, heat flux sensors, and the uncertainties in the measurement of time, density, and dimensions. The uncertainty for the heat flux sensors is determined by substituting Eq. (21) into Eq. (22). The uncertainties of the input estimates for the equipment are given in Table 1.

According to Eq. (21), the uncertainty for a single measured value of the heat flux sensors is 0.9471 W m^{-2}, and the uncertainty for single measured values of specific heat capacity and thermal conductivity are 58 J kg^{-1} K^{-1} and 0.0789 W m^{-1} K^{-1}, respectively. However, taking into account that the typical thermal conductivity of a lithium ion cell is in the range from 0.5 to 1.1 W m^{-1} K^{-1} in the considered direction, the calculated uncertainty for the single measured value of thermal conductivity is more than 5%. Therefore, repeated measurements are necessary to decrease the uncertainty of the measured parameters.

Table 1
Uncertainty of the input estimates.

Input estimates	Uncertainty of the input estimate
Time	0.1 s
34420A nanoVolt/micro-Ohm meter	70 nV/0.008 Ω (after 1 year for 23 °C ± 5 °C)
Fluke hydra series II	0.09 °C (4–Wire)
Dimensions	0.0001 m
Hear flux sensor sensitivity	$6.04 \cdot 10^{-5}$ V W^{-1} [27]
Density	0.1 kg m^{-3}

Table 2
Parameters of the test setup.

	Aluminum plate	Vacuum rubber	Fuzzed quartz
Thickness, m	0.001	0.002	0.01
Density, kg m^{-3}	2700	910	2200
Heat capacity, J kg^{-1} K^{-1}	870	2010	680
Thermal conductivity, W m^{-1} K^{-1}	205	0.13	1.35

The uncertainty for the repeated measurements is determined after the experiments by calculating the normalized standard deviation.

4. Results

The presented method was first verified on an "ideal" sample, the thermal parameters of which are well known. Fuzzed quartz with dimensions of 100 × 100 × 10 mm was chosen as the "ideal" sample. The test setup was scaled for the dimensions of the sample. The thickness and the thermal parameters of the aluminium plate, vacuum rubber, and fuzzed quartz are given in Table 2.

The minimum time of the experiment was calculated by using Eq. (15), and it is equal to 290 s. The measured temperature and heat flux on both sides on the fuzzed quartz are shown in Fig. 6.

The thermal parameters of the fuzzed quartz are calculated from 0 to 2900 s with 10 s steps in order to decrease the uncertainty of the measurements. The results of the calculation are shown in Fig. 7.

As it can be seen in Fig. 7, the deviation of the calculated values from the actual values becomes acceptable after 290 s, which is equal to the calculated value of the experiment minimum time. The thermal conductivity is equal to 1.342 ± 0.0265 W m^{-1} K^{-1}, and the specific heat capacity is equal to 706 ± 16 J kg^{-1} K^{-1}. A comparison of the average values of the thermal parameters with the actual values shows that the error for thermal conductivity is 0.58% and 3.8% for specific heat capacity. This shows the acceptability of the proposed methodology for the determination of the thermal parameters.

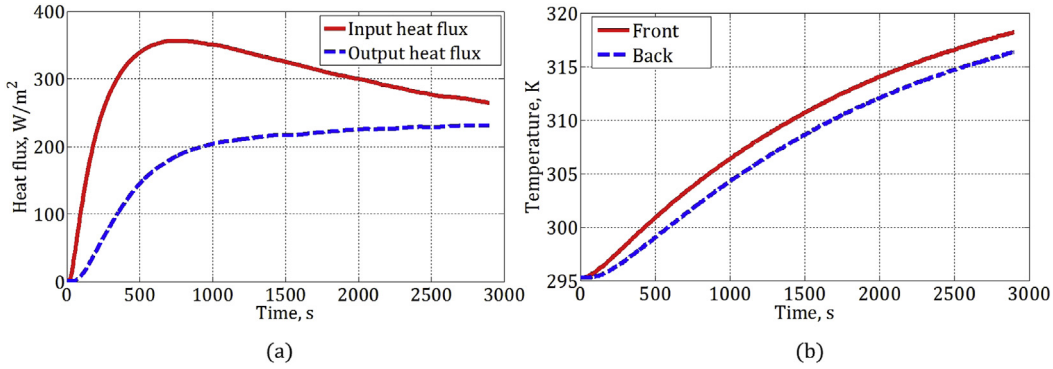

Fig. 6. Heat fluxes (a) and temperatures (b).

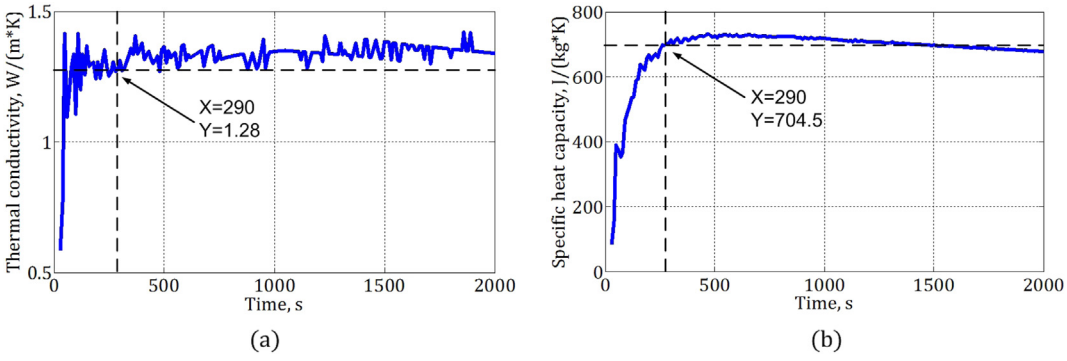

Fig. 7. Thermal conductivity (a) and specific heat capacity (b) of the quartz plate.

Table 3
Thermal parameters of the Li-ion pouch cell.

Points	Parameters	SoC				
		10%	30%	50%	70%	90%
First point	k, W m^{-1} K^{-1}	0.614 ± 0.025	0.671 ± 0.031	0.735 ± 0.034	0.704 ± 0.028	0.652 ± 0.029
	C_p, J kg^{-1} K^{-1}	1043.6 ± 12.0	1066.7 ± 9.8	1067.7 ± 9.8	1058 ± 10.5	1052.5 ± 11.2
Second point	k, W m^{-1} K^{-1}	0.633 ± 0.017	0.631 ± 0.019	0.687 ± 0.02	0.635 ± 0.02	0.594 ± 0.017
	C_p, J kg^{-1} K^{-1}	1020.7 ± 15.5	1030.1 ± 15.1	1053.7 ± 11.5	1062 ± 10.0	1052.5 ± 9.0
Third point	k, W m^{-1} K^{-1}	0.653 ± 0.021	0.647 ± 0.017	0.651 ± 0.018	0.657 ± 0.02	0.649 ± 0.022
	C_p, J kg^{-1} K^{-1}	1033.1 ± 14.0	1035.6 ± 16.1	1039.2 ± 13.9	1035.7 ± 14.4	1032.0 ± 14.9

The presented method was applied to the measurement of the thermal parameters of the Li-ion pouch cell. The thermal parameters were measured for different SoC and in different points of the cell surface, which is perpendicular to the current collectors. The SoC was varied from 10% to 90% with 20% steps. The thermal parameters were measured in three points on the cell surface with the following coordinates given in meters: (0.116, 0.216), (0.116, 0.129), and (0.116, 0.04). The results of the experiments are given in Table 3.

The minimum time of the experiment was calculated by using Eq. (15), and it is equal to 790 s. The experiments show that the specific heat capacity of the pouch Li-ion cell does not depend on the SoC, which is in compliance with [20]. The small changes in the thermal conductivity with the SoC can be explained by different amounts of particles in electrodes at different SoC. The heat is transferred in the material by chaotically moving particles, and as the operation of the Li-ion battery is based on the mass transfer, the amount of particles and the distance between them depends on the SoC. When the Li-ion battery is charged, the amount of lithium molecules increases in the negative electrode, thereby increasing the thermal conductivity of the negative electrode, which is usually lower in the considered Li-ion cell than the thermal conductivity of the negative electrode. The thermal conductivity of the positive electrode decreases because of the loss of lithium molecules. The total thermal conductivity increases and reaches its maximum value when the thermal conductivities of the electrodes are equal. If we continue charging, the total thermal conductivity starts to decrease. It can explain the parabolic dependence of the Li-ion battery on the SoC.

The dependence of the thermal parameters on the measurement points can probably be explained by the nonuniform potential distribution caused by the construction of the current collectors, which was illustrated in Ref. [15]. As the potential difference is not uniform in the electrodes, it influences the mass transfer between the electrodes. Therefore, the dependence of the thermal conductivity on the SoC is more noticeable in points that are close to the terminals of the cell, where the potential difference is higher.

5. Conclusions

A novel method for the determination of the thermal parameters of a pouch cell based on the use of gradient heat flux sensors was introduced in the paper. The method provides an opportunity to determine the through-plane thermal conductivity and the specific heat capacity by one single experiment. The method does not require a steady-state temperature mode, which makes it fast. The limitations of the method and its uncertainty were given. The method was verified by using the “ideal” sample, the thermal parameters of which are well known. The comparison of the calculated thermal parameters with actual values shows an error of 0.58% for the thermal conductivity and 3.8% for the specific heat capacity. This shows the acceptability of the method for the determination of the thermal parameters. The thermal parameters of the Li-ion pouch cell were studied by the shown method for different values of SoC and in different points on the surface. The minimum time of the experiment was calculated according presented methodology, and it is equal to 790 s for the Li-ion pouch cell used in the verification process. The experiments show that the specific heat capacity is almost independent of the SoC and the measured points. The thermal conductivity has a small parabolic dependence on the SoC, which is caused by the mass transfer between the electrodes.

References

[1] B. Scrosati, J. Garche, J. Power Sources 195 (9) (2010) 2419–2430.
[2] T. Waldmann, M. Wilka, M. Kasper, M. Fleischhammer, M. Wohlfahrt-Mehrens, J. Power Sources 262 (2014) 129–135.
[3] D. Bernardi, E. Pawlikowski, J. Newman, J. Electrochem. Soc. 132 (1) (1985) 5–12.
[4] C.R. Pals, J. Newman, J. Electrochem. Soc. 142 (10) (1995) 3274–3281.
[5] C.R. Pals, J. Newman, J. Electrochem. Soc. 142 (10) (1995) 3282–3288.
[6] Y. Chen, J.W. Evans, J. Electrochem. Soc. 140 (7) (1993) 1833–1838.
[7] Y. Chen, J.W. Evans, J. Electrochem. Soc. 141 (11) (1994) 2947–2955.
[8] S. Chen, C. Wan, Y. Wang, J. Power Sources 140 (1) (2005) 111–124.
[9] Y. Chen, J.W. Evans, J. Electrochem. Soc. 143 (9) (1996) 2708–2712.
[10] R.E. Gerver, J.P. Meyers, J. Electrochem. Soc. 158 (7) (2011) A835–A843.
[11] M. Guo, R.E. White, J. Electrochem. Soc. 158 (10) (2011) A1166–A1176.
[12] J.N. Reimers, J. Power Sources 158 (1) (2006) 663–672.
[13] K.H. Kwon, C.B. Shin, T.H. Kang, C.-S. Kim, J. Power Sources 163 (1) (2006) 151–157.
[14] U.S. Kim, C.B. Shin, C.-S. Kim, J. Power Sources 180 (2) (2008) 909–916.
[15] U.S. Kim, C.B. Shin, C.-S. Kim, J. Power Sources 189 (1) (2009) 841–846.
[16] U.S. Kim, J. Yi, C.B. Shin, T. Han, S. Park, J. Power Sources 196 (11) (2011) 5115–5121.
[17] H. Sun, X. Wang, B. Tossan, R. Dixon, J. Power Sources 206 (0) (2012) 349–356.
[18] K. Murashko, J. Pyrhonen, L. Laurila, Energy Convers. IEEE Transactions 28 (2) (2013) 335–343.
[19] H. Maleki, S.A. Hallaj, J.R. Selman, R.B. Dinwiddie, H. Wang, J. Electrochem. Soc. 146 (3) (1999) 947–954, http://dx.doi.org/10.1149/1.1391704.
[20] C. Forgez, D.V. Do, G. Friedrich, M. Morcrette, C. Delacourt, J. Power Sources 195 (9) (2010) 2961–2968.
[21] E. Barsoukov, J.H. Jang, H. Lee, J. Power Sources 109 (2) (2002) 313–320.
[22] J.P. Schmidt, D. Manka, D. Klotz, E. Ivers-Tiffe, J. Power Sources 196 (19) (2011) 8140–8146.
[23] M. Fleckenstein, S. Fischer, O. Bohlen, B. Bker, J. Power Sources 223 (0) (2013) 259–267.
[24] A.A. Pesaran, M. Keyser, in: Annual Battery Conference: Advances and Applications, 2001, pp. 1–7.
[25] A.I. Pekhovich, V.M. Zhidkikh, Calculation of the Solids Thermal Condition, second ed., Energy, Leningrad, 1976.
[26] J.H. Lienhard IV, J.H. Lienhard V, A Heat Transfer Textbook, third ed., Phlogiston Press, Cambridge, MA, U.S.A, 2008.
[27] A.V. Mityakov, S.Z. Sapozhnikov, V.Y. Mityakov, A.A. Snarskii, M.I. Zhenirovsky, J.J. Pyrhnen, Sensors Actuators A: Phys. 176 (0) (2012) 1–9.
[28] H. Jussila, A. Mityakov, S. Sapozhnikov, V. Mityakov, J. Pyrhonen, Indus. Electron. IEEE Trans. 60 (11) (2013) 4852–4860.
[29] S.Z. Sapozhnikov, V.Y. Mityakov, A.V. Mityakov, A.I. Pokhodun, N.A. S, M.S. Matveev, Meas. Tech. 54 (10) (2012) 1155–1159.